

1 **New treatment of strongly anisotropic scattering phase functions: The**
2 **Delta-M+ method**

3 Zhenyi Lin*, Nan Chen, Yongzhen Fan, Wei Li, and Knut Stamnes

4 *Department of Physics & Engineering Physics, Stevens Institute of Technology, Hoboken, NJ,*
5 *USA*

6 Snorre Stamnes

7 *NASA Langley Research Center, Hampton, VA, USA*

8 *Corresponding author address: Zhenyi Lin, Department of physics & Engineering physics,

9 Stevens Institute of Technology

10 E-mail: lzhenyi@stevens.edu

ABSTRACT

11 The treatment of strongly anisotropic scattering phase functions is still a
12 challenge for accurate radiance computations. The new Delta-M+ method
13 resolves this problem by introducing a reliable, fast, accurate, and easy-to-use
14 Legendre expansion of the scattering phase function with modified moments.
15 Delta-M+ is an upgrade of the widely-used Delta-M method that truncates
16 the forward scattering peak with a Dirac delta function, where the ‘+’ sym-
17 bol indicates that it essentially matches moments beyond the first M terms.
18 Compared with the original Delta-M method, Delta-M+ has the same com-
19 putational efficiency, but for radiance computations the accuracy and stability
20 have been increased dramatically.

21 **1. Introduction**

22 In most current scalar radiative transfer models for radiance computations in plane parallel ge-
23 ometry (Stamnes et al., 1988, 2000; Jin et al., 2006; Spurr, 2008; Rozanov et al., 2014; Lin et al.,
24 2015; Stamnes and Stamnes, 2016; Hamre et al., 2017; Stamnes et al., 2017a), the scattering phase
25 function is expanded in a finite series of Legendre polynomials. This expansion of the scattering
26 phase function combined with an expansion of the radiance in a Fourier cosine series leads to
27 a radiative transfer equation (RTE) for each Fourier component that is azimuth-independent and
28 mathematically identical for all Fourier components (Stamnes et al., 1988). As a result, an ac-
29 curate and stable RTE solution relies on an adequate expansion of the scattering phase function,
30 which could be computationally expensive, because a strongly asymmetric scattering phase func-
31 tion may require hundreds of terms in a standard Legendre polynomial expansion. For example,
32 Kokhanovsky et al. (2010) used 480 terms to expand a scattering phase function for a polydisper-
33 sion of aerosol particles and 720 terms for a polydispersion of (water) cloud droplets in order to
34 produce accurate radiative transfer benchmark results.

35 In order to alleviate the computational burden, truncation methods (Joseph et al., 1976; Wis-
36 combe, 1977; Nakajima and Tanaka, 1988; Hu et al., 2000; Mitrescu and Stephens, 2004) have
37 been introduced in which the required number of terms in the expansion is reduced by replacing
38 the sharp forward scattering peak by a Dirac delta function. Two popular truncation methods are
39 the δ -M (Wiscombe, 1977) and the δ -fit (Hu et al., 2000) methods. Overall, combined with the
40 single-scattering correction (Nakajima and Tanaka, 1988), the δ -M method, in comparison with
41 other truncations methods, was shown to provide the most accurate radiances for scattering phase
42 functions that are not too strongly forward-peaked (Rozanov and Lyapustin, 2010). The δ -M algo-

43 rithm is implemented in many radiative transfer models including DISORT (Stamnes et al., 1988)
 44 used in MODTRAN (Berk et al., 2014).

45 Nevertheless, none of the current truncation methods is perfect (Rozanov and Lyapustin, 2010).
 46 The δ -M method, designed for irradiance calculations, was found to be unable to provide accurate
 47 radiances for strongly anisotropic scattering. The δ -fit method can provide accurate radiances
 48 (except in the forward direction), but requires an *ad hoc* specification of the truncation angle
 49 and a higher computational burden than δ -M. A δ -fit user must specify by trial and error the
 50 “best” truncation angle for each scattering phase function, and the least squares fitting employed
 51 in the δ -fit method also implies additional computations. These problems make the δ -fit method
 52 inconvenient to use and slower than the δ -M method.

53 In this paper, we will address these issues by introducing a new truncation technique, the δ -M+
 54 method, designed for efficient yet accurate computation of radiances in turbid media with strongly
 55 asymmetric scattering phase functions. The new δ -M+ method represents an extension and up-
 56 grade of the standard δ -M algorithm, which leads to a significant improvement in accuracy, while
 57 retaining the same computational efficiency and “user-friendliness” as the original δ -M method
 58 (Wiscombe, 1977).

59 2. Review of the Delta-M method

60 In a full-range slab geometry the radiative transfer equation for the diffuse radiance may be
 61 written as (Stamnes et al., 2017a)

$$\begin{aligned}
 u \frac{dI(\tau, u, \phi)}{d\tau} = & I(\tau, u, \phi) - \frac{\bar{\omega}}{4\pi} \int_0^{2\pi} d\phi' \int_{-1}^1 du' p(u', \phi'; u, \phi) I(\tau, u', \phi') \\
 & - (1 - \bar{\omega})B - S^*(\tau, u, \phi),
 \end{aligned} \tag{1}$$

62 where τ is the optical depth, u is the cosine of the polar angle θ , ϕ is the relative azimuth angle,
 63 $\bar{\omega}$ is the single-scattering albedo, and $p(u', \phi'; u, \phi)$ is the scattering phase function. The term
 64 $S^*(\tau, u, \phi)$, proportional to the incident solar beam irradiance F^s , is given by

$$S^*(\tau, u, \phi) = \frac{\bar{\omega}}{4\pi} p(u', \phi'; u, \phi) F^s e^{-\tau/\mu_0} \quad (2)$$

65 where μ_0 is the cosine of the incident (solar) zenith angle. To obtain the radiance, we have to solve
 66 for a function of *three* variables, τ , u , and ϕ . But this three-variable problem can be reduced to
 67 one of solving a finite set of uncoupled radiative transfer equations, each depending on only the
 68 two variables τ and u . We start by expanding the scattering phase function in a finite series of M
 69 *Legendre polynomials* as follows ($\cos \Theta = uu' + \sqrt{1-u^2}\sqrt{1-u'^2}\cos(\phi - \phi')$):

$$p(\cos \Theta) = p(u', \phi'; u, \phi) \approx \sum_{\ell=0}^{M-1} (2\ell+1) \chi_\ell P_\ell(\cos \Theta), \quad (3)$$

70 where P_ℓ is the ℓ^{th} *Legendre polynomial*, and the ℓ^{th} expansion coefficient is given by:

$$\chi_\ell = \frac{1}{2} \int_{-1}^1 d(\cos \Theta) P_\ell(\cos \Theta) p(\cos \Theta). \quad (4)$$

71 To simplify the expansion of the scattering phase function we use the *Addition Theorem for Spher-*
 72 *ical Harmonics* (Arfken and Weber, 1999):

$$P_\ell(\cos \Theta) = P_\ell(u')P_\ell(u) + 2 \sum_{m=1}^{\ell} \Lambda_\ell^m(u')\Lambda_\ell^m(u) \cos m(\phi' - \phi) \quad (5)$$

73 where we have introduced the *normalized associated Legendre polynomial* defined by

$$\Lambda_\ell^m(u) \equiv \sqrt{\frac{(\ell-m)!}{(\ell+m)!}} P_\ell^m(u), \quad (6)$$

74 where $P_\ell^m(u)$ is the *associated Legendre polynomial*.

75 In the δ -M method, we introduce an approximate scattering phase function $p^*(\cos \Theta)$ (Wis-
 76 combe, 1977):

$$p^*(\cos \Theta) = 2f\delta(1 - \cos \Theta) + (1-f) \sum_{\ell=0}^{M-1} (2\ell+1) \chi_\ell^* P_\ell(\cos \Theta) \quad (7)$$

77 where the first term is the Dirac δ function and f is the truncation factor. The second term on the
 78 right is called the “truncated scattering phase function”, whose coefficients χ_ℓ^* are determined by
 79 matching them to the χ_ℓ of the accurate (true) scattering phase function, given by Eq. (4). This
 80 requirement leads to

$$\chi_\ell^* = \frac{\chi_\ell - f}{1 - f}, \quad \ell = 0, \dots, M - 1 \quad (8)$$

$$f = \chi_M. \quad (9)$$

81 After the truncation, the radiative transfer equation is unchanged, except that the optical depth τ
 82 and the single-scattering albedo ϖ are scaled as follows:

$$d\tau' = (1 - \varpi f)d\tau \quad (10)$$

$$\varpi' = \frac{1 - f}{1 - \varpi f} \varpi \quad (11)$$

83 where τ' and ϖ' are the scaled variables resulting from using the approximate scattering phase
 84 function in Eq. (7).

85 3. The error of the Delta-M truncation

86 Due to the orthogonality of the Legendre polynomials, the Dirac delta function in Eq. (7) may
 87 be expanded in an infinite series of Legendre polynomials:

$$2f\delta(1 - \cos \Theta) = \sum_{\ell=0}^{\infty} (2\ell + 1)fP_\ell(\cos \Theta). \quad (12)$$

88 In Eq. (12), a very important feature is the constant coefficient f for all terms in the sum. Sub-
 89 stituting Eqs. (8) and (12) into Eq. (7), we find that the approximate scattering phase function
 90 becomes:

$$p^*(\cos \Theta) = \sum_{\ell=0}^{M-1} (2\ell + 1)\chi_\ell P_\ell(\cos \Theta) + \sum_{\ell=M}^{\infty} (2\ell + 1)fP_\ell(\cos \Theta). \quad (13)$$

91 We note that the first M terms in Eq. (13) contain the standard Legendre expansion coefficients (or
 92 moments) χ_ℓ given by Eq. (4). Hence, the error incurred by applying the approximate scattering
 93 phase function is included in the higher order terms with $\ell \geq M$:

$$\varepsilon = p(\cos \Theta) - p^*(\cos \Theta) = \sum_{\ell=M}^{\infty} (2\ell + 1)(\chi_\ell - f)P_\ell(\cos \Theta). \quad (14)$$

94 Figure 1 shows an example of δ -M and δ -M+ moments (Legendre polynomial expansion co-
 95 efficients) for a H-G scattering phase function approximated by a truncated 20-term ($M = 20$)
 96 expansion. We note that the first 20 moments are accurate, but the error for higher order mo-
 97 ments ($\ell \geq 20$, shown as $\chi_\ell^* - \chi_\ell$) is much larger in the δ -M approximation than in the δ -M+
 98 approximation.

99 4. A modified representation of the Dirac delta Function

100 The δ -M method, which assumes a constant truncation for all Legendre moments, leads to large
 101 errors in higher order moments. To overcome this problem, we introduce a weighted Legendre
 102 series for the delta function as a new approximation of the Dirac delta function $\delta^*(1 - \cos \Theta)$,
 103 which we write as:

$$2f\delta^*(1 - \cos \Theta) = \sum_{\ell=0}^{\infty} (2\ell + 1)w_\ell f P_\ell(\cos \Theta) \quad (15)$$

$$w_\ell = c \cdot \exp\left(-\frac{\ell^2}{2\sigma^2}\right), \quad \ell = 0, 1, 2, \dots \quad (16)$$

104 In Eq. (15), the coefficients are changed from a constant value f to the weighted values $w_\ell f$. The
 105 purpose of introducing weights is to produce a new function that is still sharply peaked and looks
 106 close to a delta function, but also, by a suitable choice of the weights, agrees better with the actual
 107 scattering phase function for higher order moments ($\ell > M$). For simplicity, we assumed that the
 108 weights w_ℓ have a Gaussian distribution as shown in Eq. (16), where the value of c and σ are to
 109 be determined by matching $2\delta^*(1 - \cos \Theta)$ to the higher order of Legendre moments described in

110 the next section. Applying the approximate δ function given by Eq. (15), we now introduce a new,
 111 improved approximate scattering phase function, given by:

$$P_{\text{new}}^*(\cos \Theta) = 2f\delta^*(1 - \cos \Theta) + \sum_{\ell=0}^{M-1} (2\ell + 1)(\chi_\ell - w_\ell f)P_\ell(\cos \Theta). \quad (17)$$

112 Figure 1 shows how moment errors ($\chi_\ell^* - \chi_\ell$) in higher orders are reduced after using the new
 113 approximate scattering phase function (which is labeled as ‘‘New δ -M+’’).

114 One may ask what would the new approximate function $\delta^*(1 - \cos \Theta)$ look like? Figure 2 shows
 115 an example of the shape of w_ℓ and the corresponding $\delta^*(1 - \cos \Theta)$ for different combinations of
 116 c and σ . Looking at Fig. 2, we first realize that the new approximate function is normalized to
 117 w_0 , which is greater than 1.0. Therefore, it magnifies the truncation factor f in the original δ -
 118 M method. This magnification is desired because a larger forward peak truncation is needed to
 119 truncate the strongly anisotropic scattering phase function. Second, the shape of the new function
 120 just looks like a sharp spike in the forward direction, whose magnitude and width are determined
 121 by the parameters σ and c . These two parameters give us more freedom to control the sharp
 122 forward scattering peak. Third, as σ increases, the lower order moments of w_ℓ ($\ell = 0, 1, \dots, M - 1$)
 123 become closer to 1, and we see that the new approximate delta function approaches the original
 124 delta function (e.g. for $\sigma = 48$ in Fig. 2, $w_\ell \approx 1$, for $\ell = 0, 1, 2, \dots, 16$). Under this condition, the
 125 δ -M+ truncation will approach the original δ -M truncation.

126 5. The new δ -M+ method

127 Based on the new approximate Dirac delta function (Eq. (15)), we upgraded δ -M and developed
 128 a new δ -M+ truncation method. Since in Wiscombe (1977), M is essentially the order of the
 129 approximation ($M = 1$ leads to the delta-two-stream or delta-Eddington approximation), we use

130 the '+' sign to indicate an improved approximation for moments beyond the M^{th} moment by
 131 adjusting the values of the higher order weights.

132 In general, the ideal way to match higher order moments is to make every higher order term of
 133 Legendre moments correct:

$$w_\ell f = \chi_\ell, \quad \ell = M, M+1, M+2, \dots \quad (18)$$

134 However, since it is more important to get correct lower order moments than higher order ones,
 135 and since we only have two Gaussian parameters (c and σ) available to control the shape of
 136 $\delta^*(1 - \cos \Theta)$, we simply match the $(M)^{\text{th}}$ and $(M+1)^{\text{th}}$ Legendre moments by setting:

$$\begin{cases} w_M f = \chi_M \\ w_{M+1} f = \chi_{M+1}. \end{cases} \quad (19)$$

137 Note that we also define $f = \chi_M$ as in the original δ -M method so that $w_M = 1$. The solution of
 138 Eq. (19) is straightforward and given by:

$$f = \chi_M \quad (20)$$

$$w_M = 1 \quad (21)$$

$$\sigma = \sqrt{\frac{(M+1)^2 - M^2}{\ln \chi_M^2 - \ln \chi_{M+1}^2}} \quad (22)$$

$$c = w_0 = \exp\left(\frac{M^2}{2\sigma^2}\right). \quad (23)$$

139 The constant c is determined by the normalization $w_M = 1$, and $c = w_0 > 1$, which could be
 140 considered as a magnification factor of f . Next, the truncated scattering phase function in Eq. (17)

141 is normalized by dividing by $(1 - w_0 f) = (1 - f')$:

$$\chi_\ell^* = \frac{\chi_\ell - w_\ell f}{1 - f'} \quad (24)$$

$$= \frac{\chi_\ell - f' \exp(-\ell^2/2\sigma^2)}{1 - f'}, \quad \ell = 0, 1, 2, \dots, M-1 \quad (25)$$

$$f' = w_0 f = \exp(M^2/2\sigma^2) \chi_M \quad (26)$$

142 where we see that the new truncation factor $f' \geq f$.

143 At last, we need to scale the optical depth τ and the single-scattering albedo ϖ for the new
144 method in a similar manner as in the δ -M method:

$$d\tau' = (1 - \varpi f') d\tau \quad (27)$$

$$\varpi' = \frac{1 - f'}{1 - \varpi f'} \varpi. \quad (28)$$

145 6. Examples and comparison of scattering phase functions

146 a. Henyey-Greenstein scattering phase function

147 The Legendre polynomial expansion of the Henyey-Greenstein (H-G) scattering phase function
148 (Henyey and Greenstein, 1941) with asymmetry factor g is

$$p_{\text{HG}}(\cos \Theta) \approx \sum_{\ell=0}^{M-1} (2\ell + 1) g^\ell P_\ell(\cos \Theta). \quad (29)$$

149 In Figure 3, three H-G scattering phase functions with asymmetry factor $g = 0.85$ are shown in the
150 left panel: the accurate scattering phase function, δ -M truncated scattering phase function and the
151 new δ -M+ truncated scattering phase function. Sixteen terms were used to expand the truncated
152 scattering phase function. The right panel shows relative errors of the δ -M and the new δ -M+
153 scattering phase functions.

154 Except for unavoidable errors around the forward peak, the new δ -M+ scattering phase function
155 looks essentially the same as the actual (true) scattering phase function at other angles, whereas

156 the original δ -M scattering phase function fluctuates around the true scattering phase function,
157 whose relative error increases with scattering angle Θ .

158 *b. Aerosol scattering phase function*

159 To test the new δ -M+ method for large aerosol particles, we used the scattering phase function
160 adopted in Kokhanovsky's benchmark paper (Kokhanovsky et al., 2010), where a Mie code was
161 used to compute the scattering phase function at 412 nm assuming that the radius a of the aerosol
162 particles follows a lognormal distribution

$$f(a) = \frac{1}{\sqrt{2\pi}sa} \exp(-\ln^2(a/a_0)/2s^2) \quad (30)$$

163 with $a_0 = 0.2 \mu\text{m}$, $s = 0.92$ and $a_{\text{end}} = 30 \mu\text{m}$. The value of a_{end} specifies the upper limit of
164 integration of Mie optical cross section with respect to the particle radius a . The lower limit of
165 integration was equal to $0.005 \mu\text{m}$. The refractive index of the aerosol particles was set to 1.385.

166 Figure 4 shows the true, the δ -M, and the new δ -M+ scattering phase functions for this aerosol
167 case. The truncated scattering phase function is expanded using 32 terms. While the δ -M method
168 has a relative error up to 0.2 (20%), the error has been greatly reduced for the new δ -M+ method.

169 *c. Water cloud scattering phase function*

170 Similar to the aerosol test, the cloud droplet distribution from Kokhanovsky's benchmark is used
171 for the cloud case (Kokhanovsky et al., 2010). As in the aerosol case, the scattering phase function
172 was computed by a Mie code based on a narrow lognormal distribution, where $a_0 = 5 \mu\text{m}$, $s = 0.4$,
173 $a_{\text{end}} = 100 \mu\text{m}$ and the refractive index was set to $m_r = 1.339$. The maximum forward peak has a
174 very large value reaching 7,830, and there are pronounced rainbow and glory features (two more
175 peaks). We used 64 terms to expand the truncated scattering phase function. Again a comparison

176 of relative errors shows that the new δ -M+ method greatly outperforms the old method and gives
177 results with high accuracy (see Fig. 5).

178 *d. Stability test for extreme scattering phase functions*

179 We have already tested the δ -M+ method on large aerosol and water cloud particles, and reduced
180 the relative errors significantly, but we still do not know how well the δ -M+ method automatically
181 truncates extreme anisotropic scattering phase functions.

182 Two extreme scattering phase functions were introduced here based on the H-G scattering phase
183 function and the Fournier-Forand (FF) scattering phase function (Fournier and Forand, 1994). In
184 the first test we used the H-G scattering phase function with $g = 0.999$, yielding a scattering phase
185 function that is extremely forward-peaked, whose peak magnitude reaches around 2,000,000.
186 We used only 32 terms to expand the truncated scattering phase function. The results show that
187 new δ -M+ method works very well, while the original δ -M method oscillates strongly and gives
188 negative values (see Fig. 6).

189 Another sharply peaked scattering phase function is the Fournier-Forand (FF) function. We
190 adopted a refractive index (real part, $m_r = 1.0686$) typical of pigmented (phytoplankton) particles
191 and used 32 terms to test the new δ -M+ method. Again, the new method was found to work well
192 while the original δ -M method failed to converge as shown in Fig. 7.

193 *e. Ice cloud scattering phase function*

194 Finally, we tested the expansion of an ice cloud scattering phase function at $0.55\mu\text{m}$ (Takano and
195 Liou, 1989). Compared with the water cloud scattering phase function, the scattering phase func-
196 tion of ice crystals is more challenging because it has not only a stronger forward peak (reaching
197 100,000), but also halo peaks at other scattering angles which may not necessarily benefit from the

198 truncation of the forward scattering peak. As a result, hundreds of expansion terms are required
199 for accurate expanding those additional peaks even by the δ -M+ method. Applied 100 and 200
200 expansion terms we obtained the results shown in Fig. 8. We see that the Delta-M+ method has a
201 better truncation of the forward peak than the original Delta-M method, which fails to adequately
202 represent the ice crystal scattering phase function even when using 200 terms.

203 7. Radiance tests

204 From Sections 6b and 6c, it is clear that the new δ -M+ method works well and provides accurate
205 representations of the Kokhanovsky aerosol and cloud scattering phase functions. Here, we first
206 revisit these benchmarks to look at the relative error (%) of the reflectance as a function of viewing
207 polar angle. The Kokhanovsky benchmarks assume a homogeneous aerosol/cloud slab and a direct
208 beam incident at 60° at the top of the slab. The optical depth of the slab was 0.3262 for the aerosol
209 case and 5.0 for the cloud case, respectively.

210 In Fig. 9 relative errors of the Kokhanovsky aerosol benchmark results are shown for the original
211 δ -M and the new δ -M+ methods. Generally, we see that the errors have been greatly reduced
212 from 10% to less than 1% for most viewing angles. An exception happens around the exact
213 backward scattering angle ($\Delta\phi = 180^\circ, \theta = 60^\circ$). Considering that the reflectance is very small at
214 the backscattering angle, and that we used only 32 streams to compute the reflectance (instead of
215 480 in the benchmark), these errors are quite small implying that the new δ -M+ method performs
216 satisfactorily.

217 Figure 10 shows the relative errors of the Kokhanovsky cloud benchmark results. Once again,
218 the new δ -M+ method greatly reduces the relative error and provides satisfactory results.

219 Finally, a slab of particles with the extremely forward-peaked FF scattering phase function
220 shown in Fig. 7 is used to test the radiance output. The upward radiances at three azimuth an-

221 gles are shown in Fig. 11, where the incident beam angle is 30° , and the slab optical thickness
222 is set to be 0.5. The results show strong oscillations of the radiances computed with the original
223 δ -M, which could not yield converged results even for 200 streams, while the new δ -M+ method
224 provides smooth and stable results for only 32 streams.

225 **8. Summary and discussion**

226 The δ -M+ method is an enhanced version of the δ -M method that maintains the same compu-
227 tational efficiency but improves the accuracy significantly. By applying Gaussian weights $w_{\ell f}$ to
228 represent the truncation peak, the new δ -M+ method eliminates the errors of the Legendre mo-
229 ments beyond the first M expansion terms and produces accurate radiances for practical applica-
230 tions involving strongly forward-peaked scattering phase functions associated with large aerosol,
231 cloud particle, and coastal (turbid) water particles.

232 By accurately representing a majority of the Legendre moments, the δ -M+ algorithm is math-
233 ematically elegant, accurate, reliable, and computationally fast. As in the original δ -M method,
234 the truncation factor of the forward peak is automatically determined by $w_0 f$. The combination
235 of the δ -M method with the single-scattering correction can also be easily accomplished. These
236 advantages make the new δ -M+ method a practical tool that is simple and easy to implement in
237 most radiative transfer models.

238 The δ -M+ algorithm has been implemented in the latest DISORT model available at [http:](http://lllab.phy.stevens.edu/disort/)
239 [//lllab.phy.stevens.edu/disort/](http://lllab.phy.stevens.edu/disort/) (Lin et al., 2015) as well as the AccuRT model (Hamre
240 et al., 2017; Stamnes et al., 2017a).

241 Future work, aimed at improvement and extension of the new δ -M+ method, includes 1) finding
242 a possibly better weighting function to replace the simple Gaussian function; 2) testing the perfor-
243 mance of the δ -M+ method when combined with the single-scattering correction and comparing it

244 to the δ -fit and other truncation methods; and 3) applying the δ -M+ method to represent the phase
245 matrix in vector (polarized) radiative transfer models (Min and Duan, 2004; He et al., 2007; Zhai
246 et al., 2009; Cohen et al., 2013; Stamnes et al., 2017b).

247 **References**

- 248 Arfken, G. B., and H. J. Weber, 1999: *Mathematical methods for physicists*. AAPT.
- 249 Berk, A., P. Conforti, R. Kennett, and T. Perkins, Eds., 2014: *MODTRAN6: a major upgrade of*
250 *the MODTRAN radiative transfer code*, 9088H, SPIE.
- 251 Cohen, D., S. Stamnes, T. Tanikawa, E. Sommersten, J. Stamnes, J. Lotsberg, and K. Stamnes,
252 2013: Comparison of discrete ordinate and monte carlo simulations of polarized radiative trans-
253 fer in two coupled slabs with different refractive indices. *Optics express*, **21** (8), 9592–9614.
- 254 Fournier, G. R., and J. L. Forand, 1994: Analytic phase function for ocean water. *Proc. Ocean*
255 *Optics XII, SPIE*, **2558**, 194–201.
- 256 Hamre, B., S. Stamnes, K. Stamnes, and J. Stamnes, 2017: Accurt: A versatile tool for radiative
257 transfer simulations in the coupled atmosphere-ocean system. *AIP Conference Proceedings*, AIP
258 Publishing, Vol. 1810, 120002.
- 259 He, X., D. Pan, Y. Bai, Q. Zhu, and F. Gong, 2007: Vector radiative transfer numerical model of
260 coupled ocean-atmosphere system using matrix-operator method. *Science in China Series D:*
261 *Earth Sciences*, **50** (3), 442–452.
- 262 Henyey, L. G., and J. L. Greenstein, 1941: Diffuse radiation in the galaxy. *The Astrophysical*
263 *Journal*, **93**, 70–83.

- 264 Hu, Y.-X., B. Wielicki, B. Lin, G. Gibson, S.-C. Tsay, K. Stamnes, and T. Wong, 2000: δ -fit:
265 A fast and accurate treatment of particle scattering phase functions with weighted singular-
266 value decomposition least-squares fitting. *Journal of Quantitative Spectroscopy and Radiative*
267 *Transfer*, **65** (4), 681–690.
- 268 Jin, Z., T. P. Charlock, K. Rutledge, K. Stamnes, and Y. Wang, 2006: Analytical solution of
269 radiative transfer in the coupled atmosphere-ocean system with a rough surface. *Applied optics*,
270 **45** (28), 7443–7455.
- 271 Joseph, J. H., W. Wiscombe, and J. Weinman, 1976: The delta-eddington approximation for ra-
272 diative flux transfer. *Journal of the Atmospheric Sciences*, **33** (12), 2452–2459.
- 273 Kokhanovsky, A. A., and Coauthors, 2010: Benchmark results in vector atmospheric radiative
274 transfer. *Journal of Quantitative Spectroscopy and Radiative Transfer*, **111** (12), 1931–1946.
- 275 Lin, Z., S. Stamnes, Z. Jin, I. Laszlo, S.-C. Tsay, W. Wiscombe, and K. Stamnes, 2015: Improved
276 discrete ordinate solutions in the presence of an anisotropically reflecting lower boundary: up-
277 grades of the disort computational tool. *Journal of Quantitative Spectroscopy and Radiative*
278 *Transfer*, **157**, 119–134.
- 279 Min, Q., and M. Duan, 2004: A successive order of scattering model for solving vector radiative
280 transfer in the atmosphere. *Journal of Quantitative Spectroscopy and Radiative Transfer*, **87** (3),
281 243–259.
- 282 Mitrescu, C., and G. Stephens, 2004: On similarity and scaling of the radiative transfer equation.
283 *Journal of Quantitative Spectroscopy and Radiative Transfer*, **86** (4), 387–394.

- 284 Nakajima, T., and M. Tanaka, 1988: Algorithms for radiative intensity calculations in moderately
285 thick atmospheres using a truncation approximation. *Journal of Quantitative Spectroscopy and*
286 *Radiative Transfer*, **40** (1), 51–69.
- 287 Rozanov, V., A. Rozanov, A. Kokhanovsky, and J. Burrows, 2014: Radiative transfer through ter-
288 restrial atmosphere and ocean: software package sciatran. *Journal of Quantitative Spectroscopy*
289 *and Radiative Transfer*, **133**, 13–71.
- 290 Rozanov, V. V., and A. I. Lyapustin, 2010: Similarity of radiative transfer equation: Error analysis
291 of phase function truncation techniques. *Journal of Quantitative Spectroscopy and Radiative*
292 *Transfer*, **111** (12), 1964–1979.
- 293 Spurr, R., 2008: Lidort and vlidort: Linearized pseudo-spherical scalar and vector discrete ordinate
294 radiative transfer models for use in remote sensing retrieval problems. *Light Scattering Reviews*
295 **3**, Springer, 229–275.
- 296 Stamnes, K., and J. J. J. Stamnes, 2016: *Radiative transfer in coupled environmental systems: an*
297 *introduction to forward and inverse modeling*. John Wiley & Sons.
- 298 Stamnes, K., G. E. Thomas, and J. J. Stamnes, 2017a: *Radiative transfer in the atmosphere and*
299 *ocean*. Cambridge University Press, second edition.
- 300 Stamnes, K., S.-C. Tsay, W. Wiscombe, and K. Jayaweera, 1988: Numerically stable algorithm for
301 discrete-ordinate-method radiative transfer in multiple scattering and emitting layered media.
302 *Applied optics*, **27** (12), 2502–2509.
- 303 Stamnes, K., S.-C. Tsay, W. Wiscombe, and I. Laszlo, 2000: Disort, a general-purpose fortran
304 program for discrete-ordinate-method radiative transfer in scattering and emitting layered me-

305 dia: documentation of methodology. Tech. rep., Tech. rep., Dept. of Physics and Engineering
306 Physics, Stevens Institute of Technology, Hoboken, NJ 07030.

307 Stamnes, S., S. Ou, Z. Lin, Y. Takano, S. Tsay, K. Liou, and K. Stamnes, 2017b: Polarized radia-
308 tive transfer of a cirrus cloud consisting of randomly oriented hexagonal ice crystals: The 3×3
309 approximation for non-spherical particles. *Journal of Quantitative Spectroscopy and Radiative*
310 *Transfer*, **193**, 57–68.

311 Takano, Y., and K.-N. Liou, 1989: Solar radiative transfer in cirrus clouds. part i: Single-scattering
312 and optical properties of hexagonal ice crystals. *Journal of the Atmospheric Sciences*, **46 (1)**,
313 3–19.

314 Wiscombe, W., 1977: The delta-m method: rapid yet accurate radiative flux calculations for
315 strongly asymmetric phase functions. *Journal of the atmospheric sciences*, **34 (9)**, 1408–1422.

316 Zhai, P.-W., Y. Hu, C. R. Trepte, and P. L. Lucker, 2009: A vector radiative transfer model for
317 coupled atmosphere and ocean systems based on successive order of scattering method. *Optics*
318 *express*, **17 (4)**, 2057–2079.

319 **LIST OF TABLES**

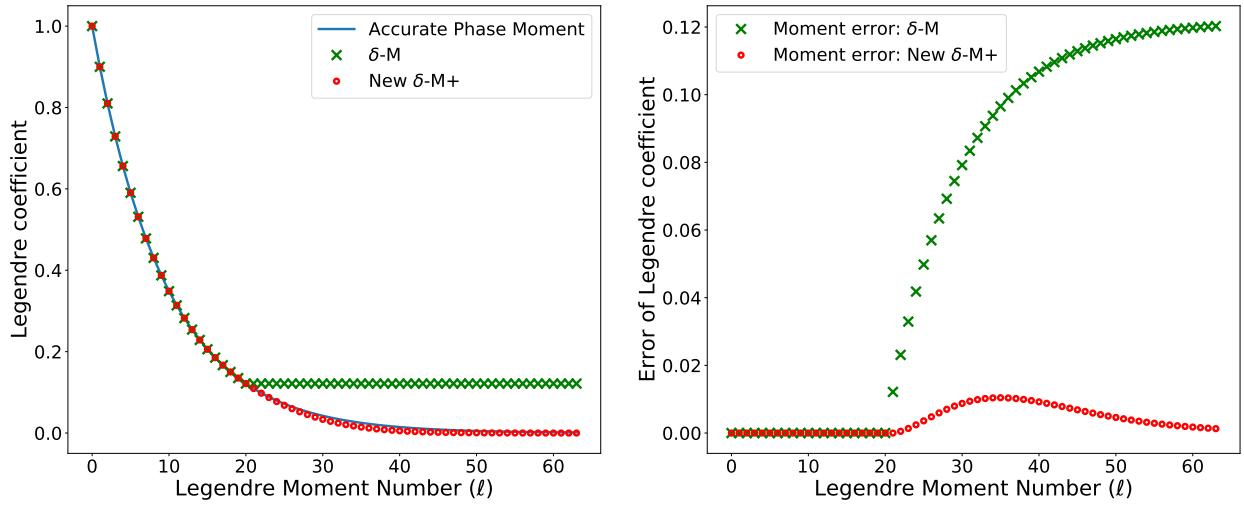
320 **Table 1.** Magnitude of the σ and c parameters of the δ -M+ in Figures 3-8. 20

TABLE 1. Magnitude of the σ and c parameters of the δ -M+ in Figures 3-8.

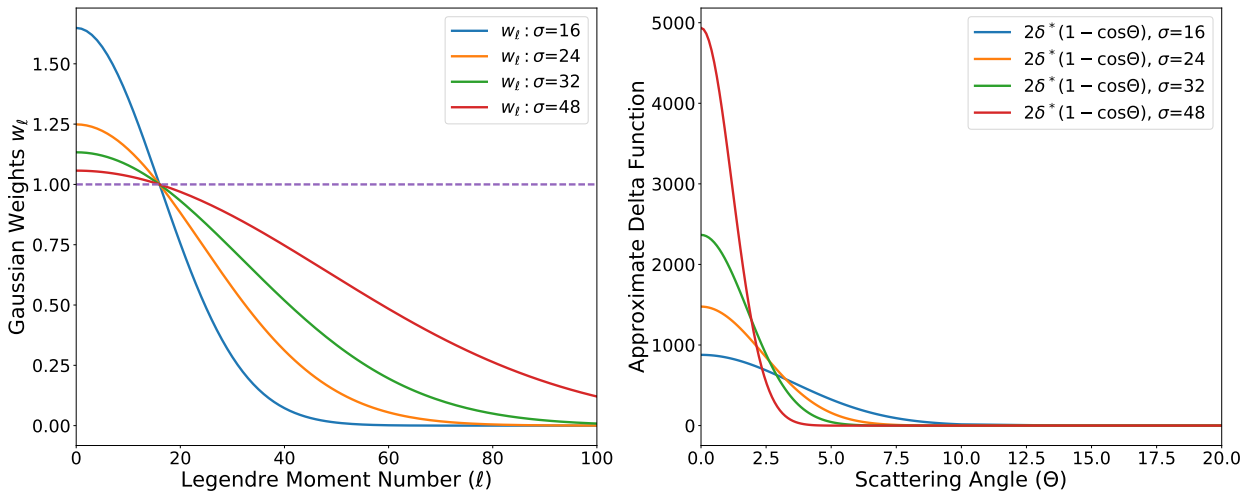
Figure no.	σ	c
3	10.076	3.528
4	31.700	1.664
5	80.903	1.367
6	180.232	1.016
7	51.749	1.211
8 (100 terms)	162.532	1.208
8 (200 terms)	217.710	1.525

LIST OF FIGURES

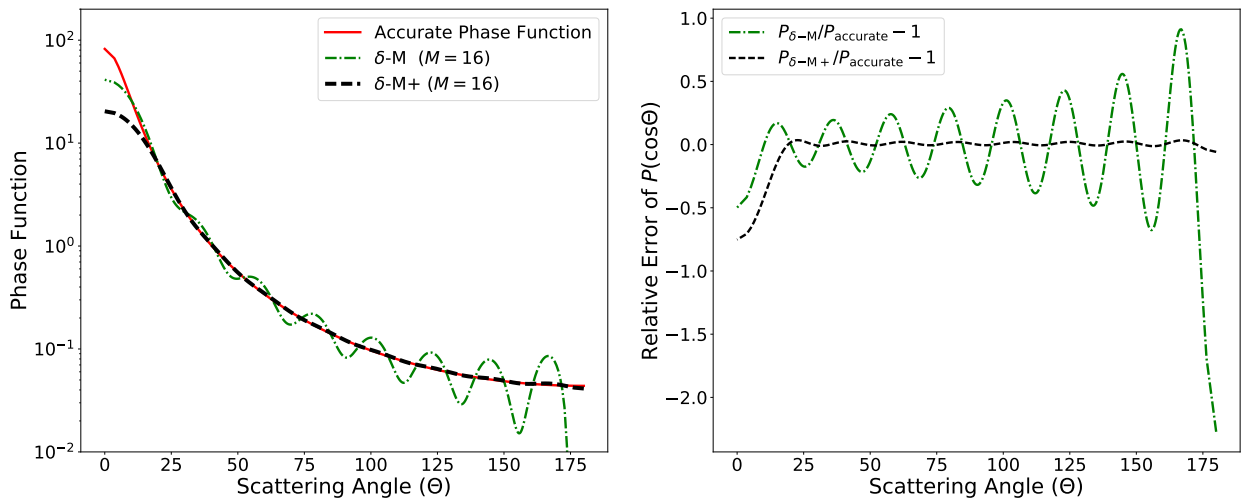
321		
322	Fig. 1.	Moments (left) and moment errors (right) of a 20-term δ -M and δ -M+ representation of a
323		H-G scattering phase function with asymmetry factor $g = 0.9$ 22
324	Fig. 2.	Gaussian weights and corresponding new approximate delta function $\delta^*(1 - \cos \Theta)$, where
325		c is determined by normalizing $w_{16} = 1$. The horizontal dashed line corresponds to the
326		condition without weighting ($w_\ell = 1$). 23
327	Fig. 3.	H-G scattering phase function ($g = 0.85$). 16 terms are used for the Legendre polynomial
328		expansion of the δ -M and the new δ -M+ method. The magnitude of the parameters σ and c
329		are listed in Table 1. 24
330	Fig. 4.	Kokhanovsky's aerosol scattering phase function. 32 terms are used for the Legendre poly-
331		nomial expansion of the δ -M and new δ -M+ methods. The magnitude of the parameters σ
332		and c are listed in Table 1. 25
333	Fig. 5.	Kokhanovsky's cloud scattering phase function. 64 terms are used for the Legendre poly-
334		nomial expansion of the δ -M and new δ -M+ methods. The magnitude of the parameters σ
335		and c are listed in Table 1. 26
336	Fig. 6.	H-G scattering phase function ($g = 0.999$). 32 terms are used for the Legendre polynomial
337		expansion of the δ -M and the new δ -M+ methods. The magnitude of the parameters σ and
338		c are listed in Table 1. 27
339	Fig. 7.	FF scattering phase function ($m_r = 1.0686$). 32 terms are used for the Legendre polynomial
340		expansion of the δ -M and the new δ -M+ methods. The magnitude of the parameters σ and
341		c are listed in Table 1. 28
342	Fig. 8.	Ice cloud scattering phase function expanded by 100 terms (left) and 200 terms (right). The
343		magnitude of the parameters σ and c are listed in Table 1. 29
344	Fig. 9.	Relative error (%) for the Kokhanovsky aerosol benchmark. 30
345	Fig. 10.	Relative error (%) for the Kokhanovsky cloud benchmark. 31
346	Fig. 11.	Upward radiance from a homogeneous layer with a FF scattering phase function. 32



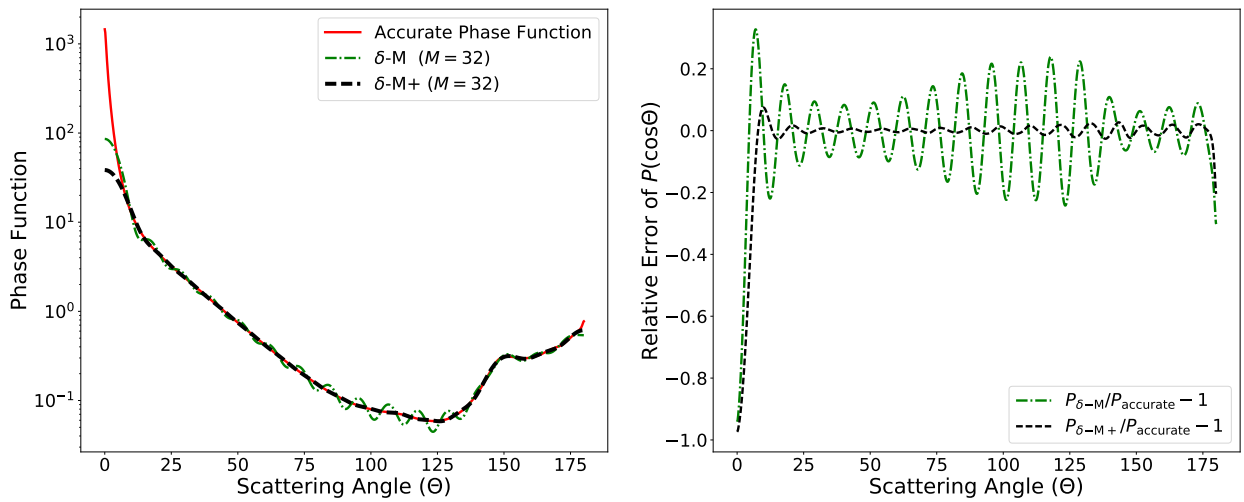
347 FIG. 1. Moments (left) and moment errors (right) of a 20-term δ -M and δ -M+ representation of a H-G
 348 scattering phase function with asymmetry factor $g = 0.9$.



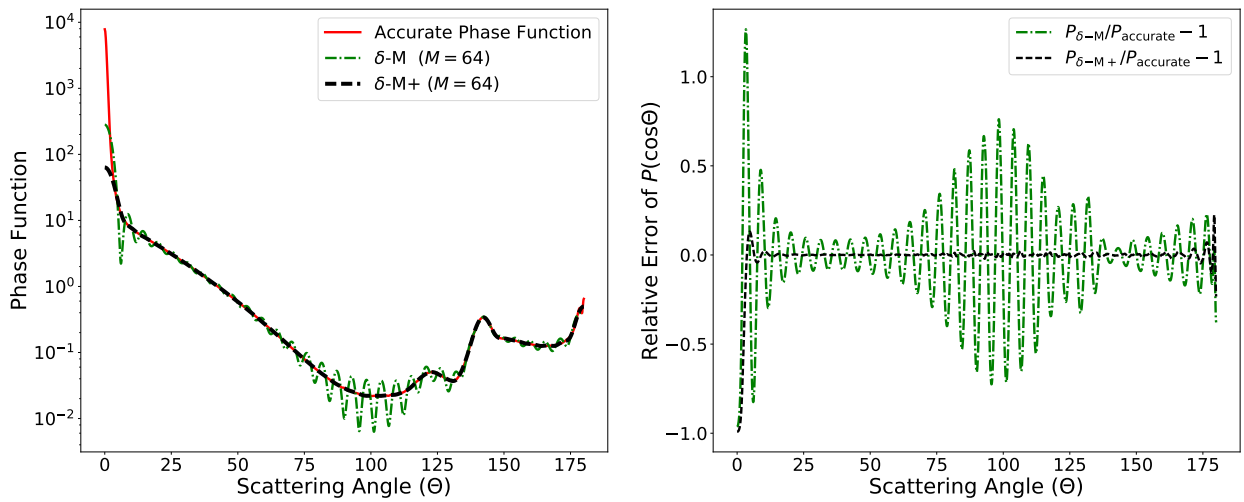
349 FIG. 2. Gaussian weights and corresponding new approximate delta function $\delta^*(1 - \cos\Theta)$, where c is de-
 350 termined by normalizing $w_{16} = 1$. The horizontal dashed line corresponds to the condition without weighting
 351 ($w_\ell = 1$).



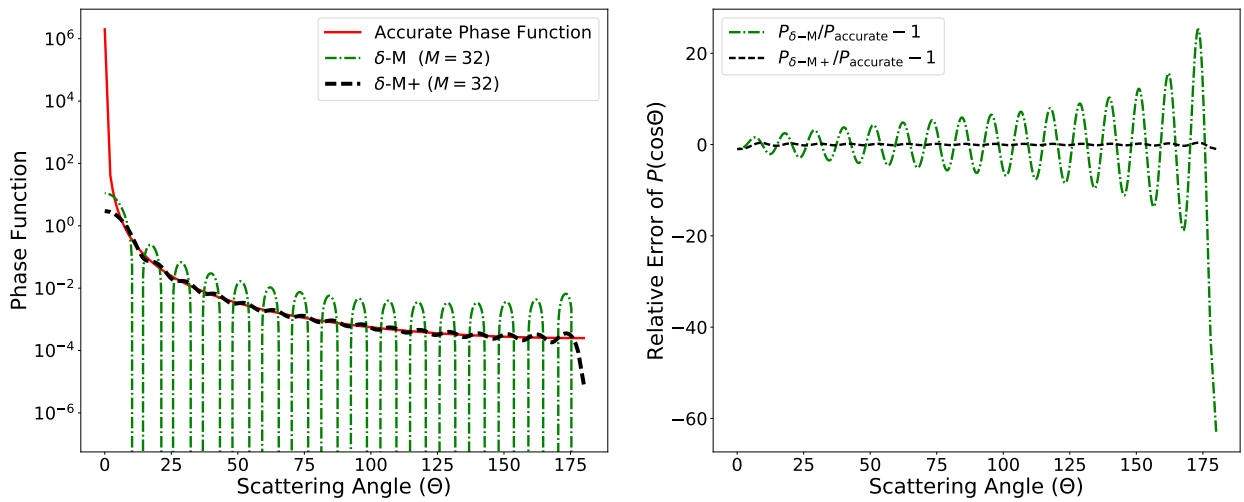
352 FIG. 3. H-G scattering phase function ($g = 0.85$). 16 terms are used for the Legendre polynomial expansion
 353 of the δ -M and the new δ -M+ method. The magnitude of the parameters σ and c are listed in Table 1.



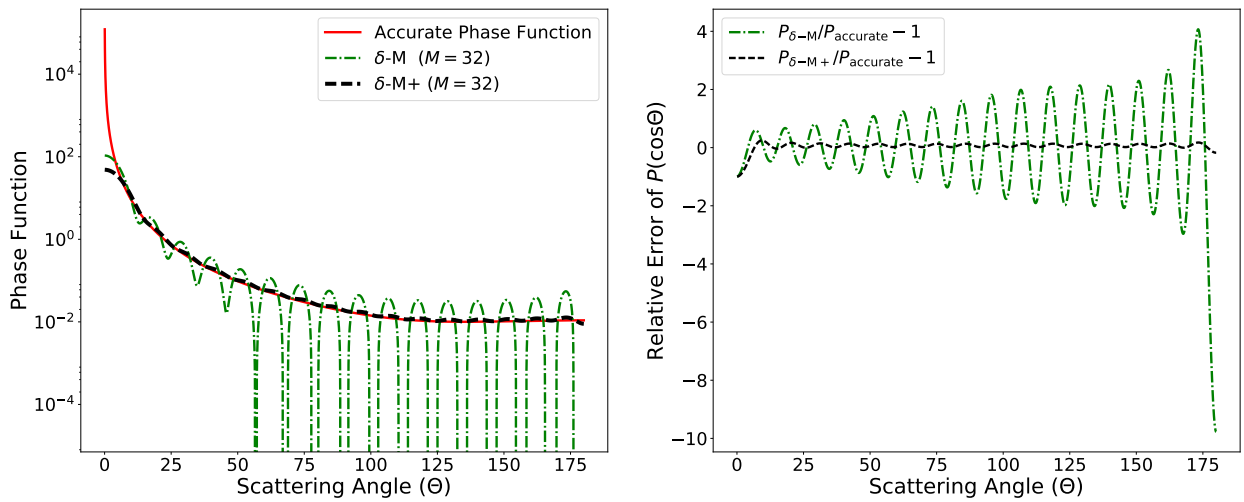
354 FIG. 4. Kokhanovsky's aerosol scattering phase function. 32 terms are used for the Legendre polynomial
 355 expansion of the δ -M and new δ -M+ methods. The magnitude of the parameters σ and c are listed in Table 1.



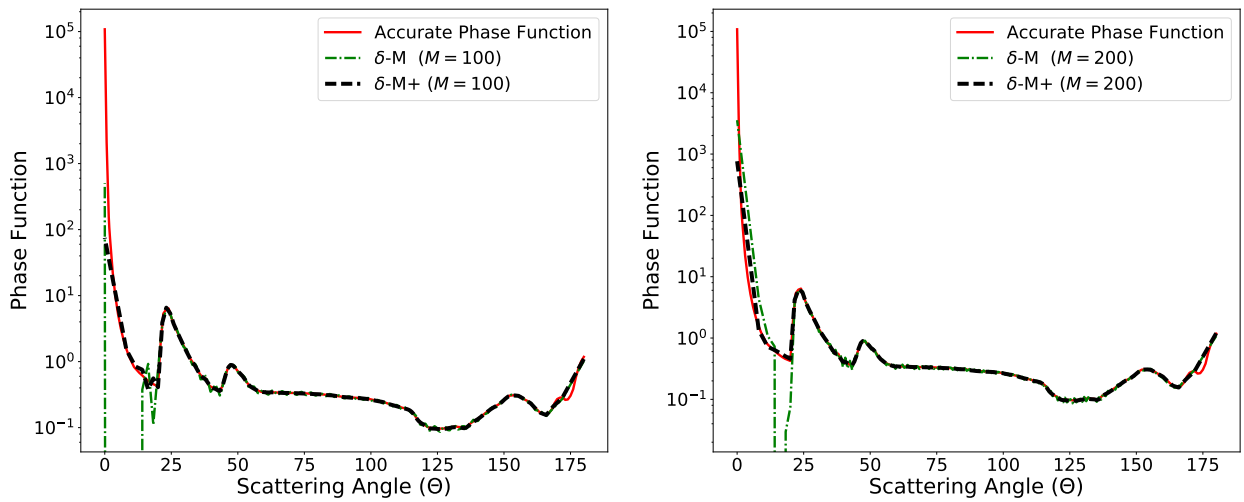
356 FIG. 5. Kokhanovsky's cloud scattering phase function. 64 terms are used for the Legendre polynomial
 357 expansion of the δ -M and new δ -M+ methods. The magnitude of the parameters σ and c are listed in Table 1.



358 FIG. 6. H-G scattering phase function ($g = 0.999$). 32 terms are used for the Legendre polynomial expansion
 359 of the δ -M and the new δ -M+ methods. The magnitude of the parameters σ and c are listed in Table 1.



360 FIG. 7. FF scattering phase function ($m_r = 1.0686$). 32 terms are used for the Legendre polynomial expansion
 361 of the δ -M and the new δ -M+ methods. The magnitude of the parameters σ and c are listed in Table 1.



362 FIG. 8. Ice cloud scattering phase function expanded by 100 terms (left) and 200 terms (right). The magnitude
 363 of the parameters σ and c are listed in Table 1.

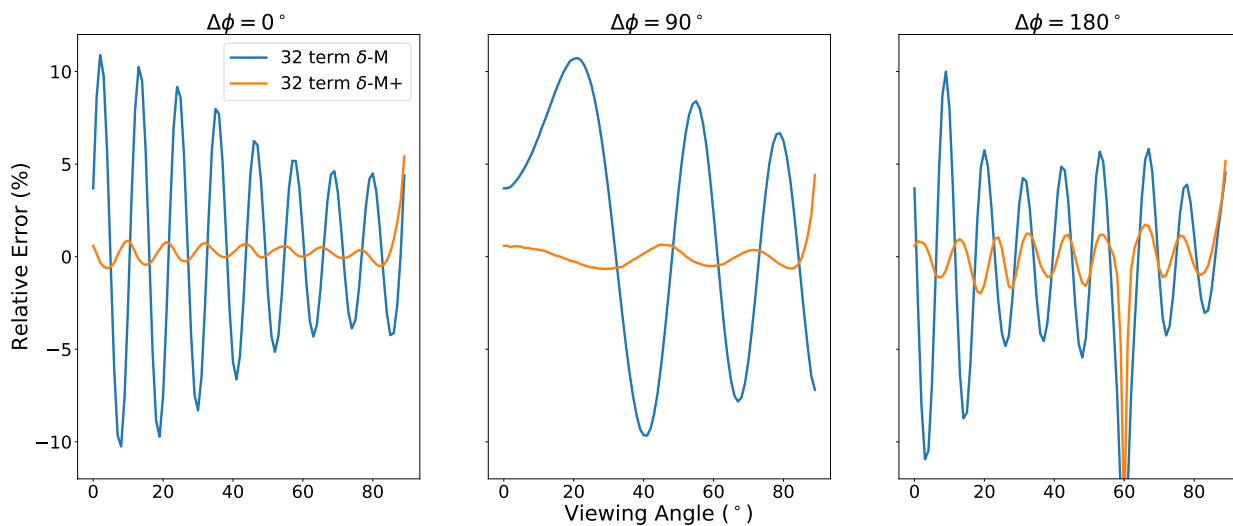


FIG. 9. Relative error (%) for the Kokhanovsky aerosol benchmark.

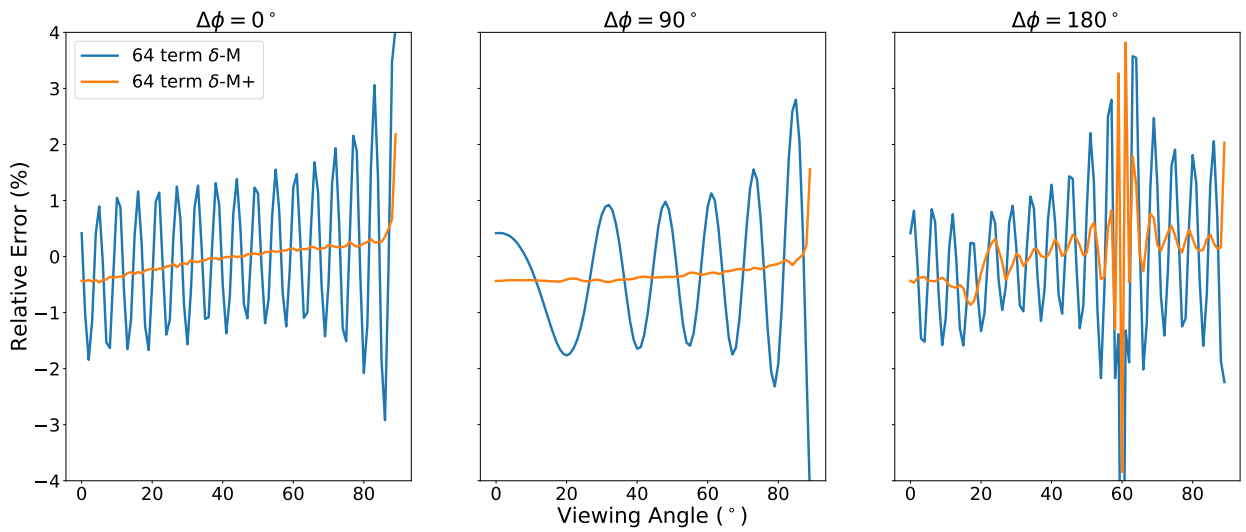


FIG. 10. Relative error (%) for the Kokhanovsky cloud benchmark.

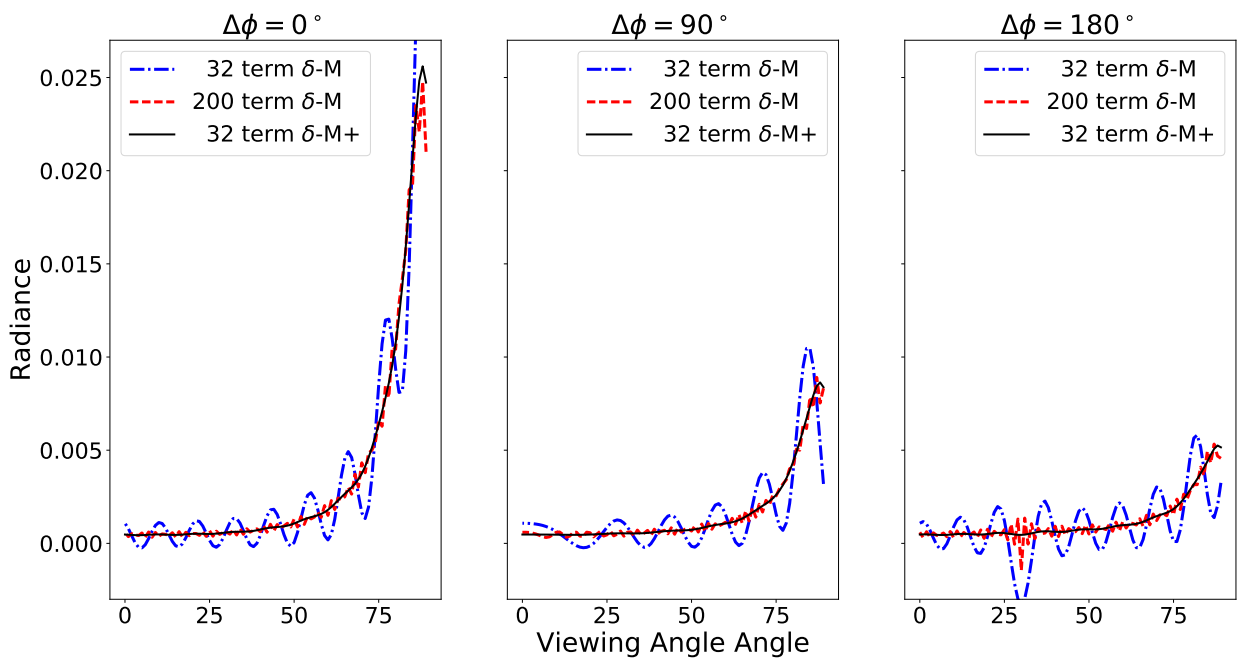


FIG. 11. Upward radiance from a homogeneous layer with a FF scattering phase function.